Quaternary Science Reviews 376 (2026) 109816

Contents lists available at ScienceDirect

Quaternary Science Reviews

journal homepage: www.elsevier.com/locate/quascirev

New evidence for a 179 ka age of the Old Crow tephra

Desmond Yeo [a,b,*], Yongsong Huang [a,**], Fei Guo [c], Richard S. Vachula [d], Karen J. Wang [a], Jonathan A. O'Donnell [e], Steven C. Clemens [a,b], James M. Russell [a,b]

[a] Department of Earth, Environmental and Planetary Sciences, Brown University, 324 Brook Street, Providence, RI, 02912, USA
[b] Institute at Brown for Environment and Society, Department of Earth, Environmental, and Planetary Sciences, Brown University, Providence, RI, 02912, USA
[c] State Key Laboratory of Loess Science, Institute of Earth Environment, Chinese Academy of Sciences, Xi'an, 710061, China
[d] Department of Geosciences, Auburn University, 2050 Beard-Eaves Memorial Coliseum, Auburn, AL, 36849, USA
[e] National Park Service, Arctic Network, 240 W 5th Ave, Anchorage, AK, 99501-2327, USA

ARTICLE INFO

Handling editor: Biagio Giaccio

Keywords:
Pleistocene
Paleolimnology
Arctic
Imuruk
Tephrochronology
Quaternary stratigraphy

ABSTRACT

Accurate age control is a prerequisite for paleoclimate and paleoenvironmental research but remains a persistent challenge for Arctic lake sediment cores. Well-dated regional tephrochronologies can provide robust stratigraphic markers in sediments. In Arctic Eastern Beringia, the Old Crow tephra (OCt) is one of the most widely distributed late Quaternary tephras and serves as an important stratigraphic anchor beyond the radiocarbon range (>50 ka BP). However, the age of the OCt remains debated and has undergone numerous revisions, with studies using different dating methodologies to ascribe ages ranging from 124 ka to 203 ka. While the commonly reported age of the OCt based on fission track dating is 124 ± 10 ka, a recent study using uranium-thorium/helium ((U-Th)/He) dating of zircon placed the OCt at 202.9 ± 9.5 ka. Here, we independently find an age of 179.0 ± 4.6 ka for the OCt from a lacustrine sediment record in Alaska (Imuruk Lake) with confirmation using the marine benthic $\delta^{18}O$ chronology. This revises the current tephrostratigraphic framework in this region. We also report a previously undocumented mafic tephra layer (IM#1), which is likely a local eruption on the Seward Peninsula, with an age of 157.2 ± 4.7 ka, providing a new tephrostratigraphic marker for this region.

1. Introduction

Explosive volcanic eruptions produce large amounts of tephra, which can be ejected high into the atmosphere and deposited hundreds to thousands of kilometers away. Such widespread tephra dispersion has been recorded worldwide in areas of active volcanic activity spanning the globe (Bogaard and Schmincke, 1985; Lowe et al., 2008). For example, the 1815 Tambora eruption ejected approximately 150 km^3 of ash spreading over a distance of at least 1300 km, resulting in global cooling and the "year without a summer" in Europe (Brönnimann and Krämer, 2016; Stothers, 1984). As volcanic eruptions disperse ash simultaneously across broad regions, tephra layers provide isochronous markers that enable stratigraphic correlation between geographically disparate sedimentary records (Burgess et al., 2019).

In the Arctic, tephrostratigraphy is particularly important for dating late Quaternary sediment cores. This is because sedimentary organic matter in Arctic lakes is often anomalously old due to slow degradation rates of organic matter by microbes at low temperatures, resulting in long residence time in soils and lake sediments (Longman et al., 2021; Strauss et al., 2015), limiting the effectiveness of carbon-based chronometers. Additionally, there are often sedimentary hiatuses due to geomorphological processes associated with glacial cycles, which often complicates chronological interpolation between dated beds (Alexanderson et al., 2014). Consequently, large distal eruptions originating from the Aleutian volcanic arc has provided critical chronological anchors for sediments in Eastern Beringia. Key examples include several notable Late Pleistocene tephra layers such as the Dawson tephra (Froese et al., 2002), OCt (Preece et al., 2011), Sheep Creek tephra (SCt) (Berger et al., 1996; Westgate et al., 2008) and the Variegated tephra (Vt) (Jensen et al., 2011), which have been widely used as important chronostratigraphic markers for paleoclimate and paleoenvironmental studies.

The OCt is a highly distinctive tephra and one of the most important chronological anchors in Eastern Beringia, with a presumed source crater at Emmons Lake (Preece et al., 2011). It was first documented at the Old Crow lowlands of Yukon territory, but has also been recorded in

* Corresponding author. Department of Earth, Environmental and Planetary Sciences, Brown University, 324 Brook Street, Providence, RI, 02912, USA.
** Corresponding author.
E-mail addresses: desmondyeo@brown.edu (D. Yeo), Yongsong_huang@brown.edu (Y. Huang).

https://doi.org/10.1016/j.quascirev.2026.109816
Received 12 January 2026; Accepted 16 January 2026
Available online 27 January 2026
0277-3791/© 2026 The Authors. Published by Elsevier Ltd. This is an open access article under the CC BY license (http://creativecommons.org/licenses/by/4.0/).

the Seward Peninsula, Wrangell Mountains, and in interior Alaskan (Westgate et al., 1983). OCt deposits are extensively distributed in Eastern Beringia as a prominent layer of white ash, typically 5–20 cm thick (Begét et al., 1991; Westgate et al., 1985). The thickest deposit of the OCt (20 cm) was recorded at the Palisades along the Yukon River in Alaska (Begét et al., 1991). OCt glass shards are mostly clear, with bubble-wall-like fragments and have a high silica glass composition (Preece et al., 2011; Westgate et al., 1983). Its distinctive appearance, uniform elemental composition, and widespread spatial distribution suggest that it originated from a single large eruption from the Aleutian arc (Preece et al., 2011).

The eruption age of the OCt has been dated using a variety of techniques. Early work using fission-track dating yielded an age of 140 ± 10 ka (Westgate et al., 1990). The age was further constrained to 131 ± 11 ka also using fission-track dating, with the inclusion of supplementary samples of the OCt from Togiak Bay, Alaska (Péwé et al., 2009). Additional fission-track dating has resulted in a now widely reported age of 124 ± 10 ka (Preece et al., 2011). However, fission-track dating is prone to bias as partial annealing can yield younger-than-eruption ages, while the misidentification of microlite inclusions can produce older ages (Walter, 1989). A recent study using (U-Th)/He dating on zircon reported an older age of 202.9 ± 9.5 ka (Burgess et al., 2019). Zircon (U–Th)/He dates record cooling below ~250 °C, which corresponds to eruption and deposition, rather than crystallization. Burgess et al. (2019) also reported concordance between zircon U–Th/He, U–Pb, and U-series ages, suggesting an eruption age estimate of ~203 ka. Furthermore, the detrital grains of OCt were recently found in a marine sediment core IODP Site U1345 from the Bering Sea across several series of discrete layers, suggesting a minimum age of 159 ± 8 ka (Reyes et al., 2023). Site U1345 contains a high sedimentation sequence (Jang et al., 2017; Kender and Kaminski, 2017) with a benthic foraminiferal $\delta^{18}O$ record that can be aligned to regional North Pacific stratigraphy to provide an independent framework for evaluating the age of the OCt. The wide range of reported ages based on different dating approaches (i.e., fission track 124 ± 10 ka, (U-Th)/He, U-series, U-Pb 202.9 ± 9.5 ka, marine sediment >159 ± 8 ka) for the OCt results in major uncertainties regarding the use of this prominent tephra layer as a chronological datum in eastern Beringia.

In this study, we build upon the chronology of Guo et al. (2025) by integrating radiocarbon and paleomagnetic ages into a Bayesian age-depth model, constraining the eruption age of the OCt to 179.0 ± 4.6 ka. We do so by 1) using a new and independently dated sediment core from Imuruk Lake, Alaska, to constrain the age of the OCt and 2) corroborating the Imuruk Lake-based age using the benthic marine $\delta^{18}O$ stratigraphy by comparing the chemical composition of the OCt in Imuruk Lake sediments with published data from IODP Site U1345. In addition, we identified a previously undocumented local mafic tephra layer in the Imuruk sequence, which we named IM#1 and describe in this study.

2. Regional setting

Imuruk Lake (65.58°N, 163.22°W; 290 m a.s.l) is a large freshwater lake located in the center of the Seward Peninsula, Alaska. It has a surface area of 80 km^2 and is the largest lake in Eastern Beringia. The lake occupies a structural basin within a volcanic province and is mostly underlain by Quaternary basaltic lava flows (Hopkins, 1949). Modern prevailing surface winds in Alaska exhibit a bimodal regime, characterized by northeasterlies during winter and southwesterlies during summer (Muhs and Budahn, 2006).

Arctic lakes serve as important archives of volcanic eruptions in Eastern Beringia and can document the age and provenance of tephra. However, the preservation of tephras older than the last ice age in Arctic lakes remains a challenge because most lakes were glaciated or desiccated during the Last Glacial Maximum (LGM) ca. 21.5 ka (Vachula et al., 2019). Tephra in Eastern Beringia may derive from several volcanic provinces, which includes the Imuruk volcanic field on the Seward Peninsula and the Emmons Lake on the east Aleutian arc, the latter of which is the hypothesized source of the OCt (Preece et al., 2011). Many important tephra anchors have been found in loess deposits across interior Alaska and the Yukon, such as the Dawson tephra (central Yukon) (Froese et al., 2002), the OCt (interior Alaska and the Yukon) (Preece et al., 2011), the Sheep Creek tephra (SCt) (central Alaska and the Yukon) (Berger et al., 1996) and the Variegated tephra (a key MIS 5 marker) (Vt) (Jensen et al., 2011). These regional tephra anchors have served as valuable tie points for correlating sediment sequences across Beringia. Site U1345 is a continental slope sediment core from the northern Bering Sea that preserves a continuous Pleistocene sequence with well resolved benthic foraminiferal $\delta^{18}O$ stratigraphy (Reyes et al., 2023; Worne et al., 2019). Amongst other marine sites in the Bering Sea, Site U1345 is of interest as shards of OCt have been found from the site (Reyes et al., 2023).

Imuruk Lake's location on the Seward Peninsula makes it an ideal archive of volcanic eruptions in the region, such as those from the Imuruk volcanic field, and larger eruptions originating from the distal Aleutian Arc. More importantly, Imuruk Lake persisted during the LGM, thus ensuring a continuous sedimentary record. Fig. 1 depicts the current documented extent of the OCt from the presumed source crater at Emmons Lake (Preece et al., 2011), as well as the various marine sites of interest reported in Reyes et al. (2023). The dashed outline represents the distribution of the OCt inferred from presently known outcrops and thickness measurements (Burgess et al., 2019; Froese et al., 2002). It is not intended to mark a fixed boundary as additional OCt sites beyond this boundary may be identified with future sampling.

3. Material and methods

3.1. Sample preparation

The Imuruk Lake core was obtained using a Livingstone corer attached to a winch system during a field campaign in April 2019. Two parallel sediment cores were collected from Imuruk Lake at the same location. Together, the two cores accounted for 28 physical core sections, each approximately 0.5 m long. Each section was split lengthwise into an archive half for XRF scanning, and a working half for geochemical and biomarker analysis. Photographs of the core were taken using a Geotek Multi-Sensor Core Logger (MSCL-S) core scanner at the Continental Scientific Drilling Facility at the University of Minnesota. The 28 core sections were scanned and sampled at a resolution of 1 cm for geochemical and physical measurements. Finally, we composited the two parallel cores to a common depth scale using high-resolution rubidium/strontium (Rb/Sr) and core imagery to obtain an 8.8 m sedimentary sequence.

Two tephra beds were identified in the core. Bed A is located at a depth of 648 cm bisected by a visually clear 0.2 cm thick layer of grayish sediment. Bed B is located at a depth of 735 cm (Fig. S1). Bed B occurs as a distinct ash layer characterized by a light gray color, sharp upper and lower contacts, with a thickness of ~1.5 cm. These physical characteristics and its stratigraphic position prompted further geochemical investigation to determine whether Bed B corresponds to the Old Crow tephra.

3.2. Electron probe microanalysis (EPMA)

Tephra beds A and B were sampled using a small stainless-steel spatula pre-cleaned with Kimwipes and methanol. Analyses were conducted on Bed B samples at the Electron Microprobe Facility at Brown University. Preliminary microscopic observation of Bed B confirmed that glass was relatively pure and abundant, with over 90 % glass and the remaining fraction consisting of minor mineral grains and lithic fragments (Fig. S2a). To prepare the samples for EPMA, two one-inch hollow polycarbonate cylinders were mounted on a double-sided tape

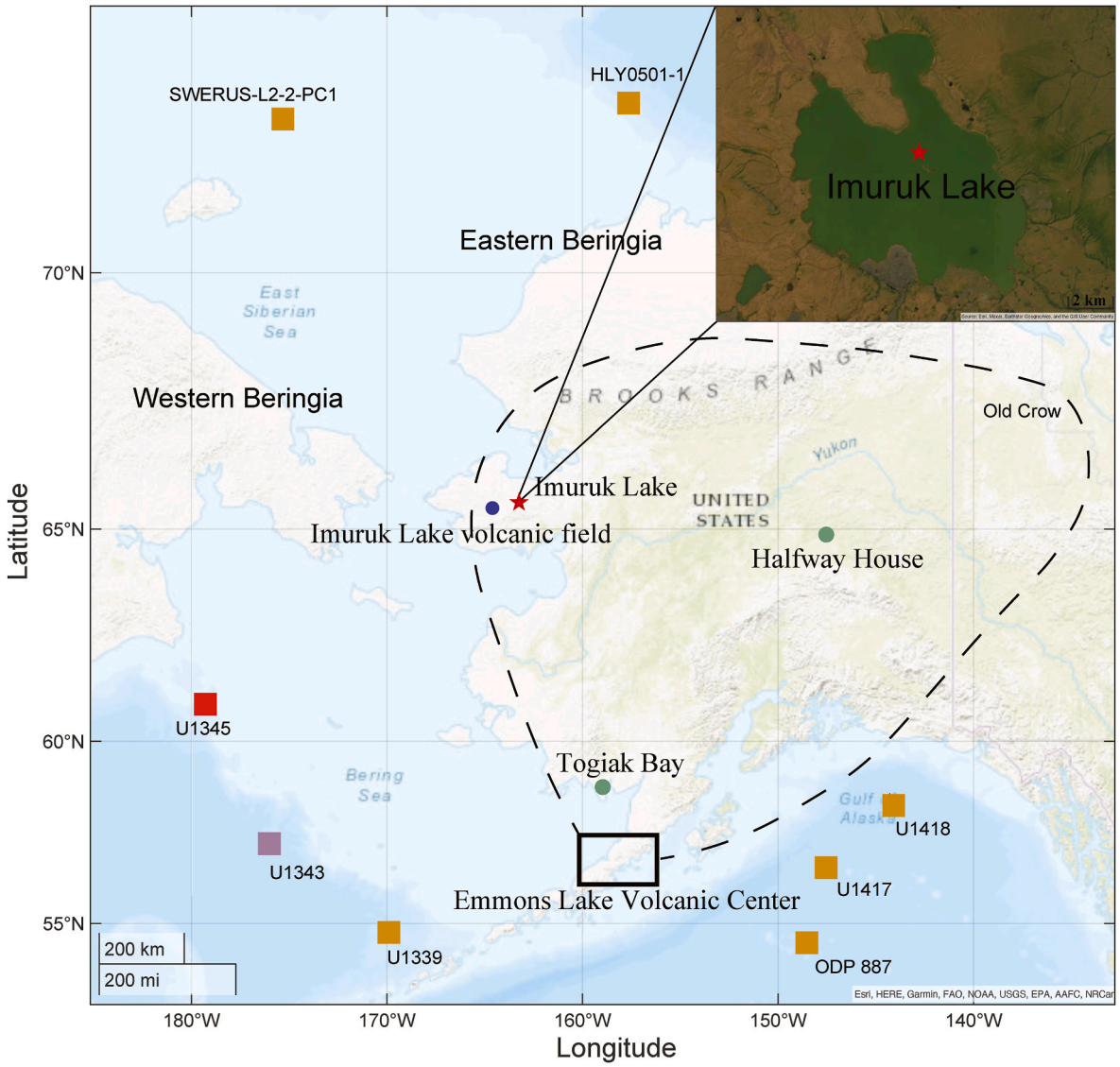


Fig. 1. Map of Eastern Beringia showing the currently documented extent of the OCt (Burgess et al., 2019; Froese et al., 2002). The location of the study site is labelled with a red star (the inset shows a satellite image of Imuruk Lake). The Emmons Lake volcanic center (presumed source crater of the OCt) is marked with a black rectangle (Preece et al., 2011). The blue circle represents the Imuruk volcanic field, a hypothesized source region for IM#1. Marine sites examined by Reyes et al. (2023) are indicated by brown squares, while Site U1345 where detrital shards of OCt were found, is indicated by the red square. The age model of Site U1343 (indicated by the purple square) was used to revise Site U1345's age model. Green circles indicate the Halfway House and Togiak Bay sites, where the OCt has been extensively documented in the literature, with thicknesses of 30 and 40 cm, respectively (Jensen et al., 2016; Péwé et al., 2009).

and the samples were sprinkled in from the top and the cylinder was filled with epoxy. The epoxy was cured using a hotplate and polished. Quantitative analyses of glass were performed using a Cameca SX-100 electron microprobe. The operating conditions of the instrument consisted of 15 kV voltage, 10 nA current and a 10-μm diameter defocused beam. Counting times for all elements were 30 s on peak, and for backgrounds, except Na (peak = 20 s). The data were calculated using the PAP correction procedures (Pouchou and Pichoir, 1991). One-sigma standard deviations were <1 % for major elements and 3–12 % for minor elements. The standards used for major and minor element calibration included USGS KN18B rhyolite glass, University of Rhode Island (Si); USGS BIR-1G Iceland basalt glass (Ca, Al); synthetic Fo97 forsterite, University of Rhode Island (Mg); Rockport, Massachusetts fayalite; NMNH 85276 (Fe); Amelia albite, Purdue University (Na); rhodonite, AMNH 104738 (Mn); synthetic orthoclase OR-1, AMNH (K); synthetic berlinite, AMNH (P); synthetic rutile, Brown University, (Ti); synthetic $MgCr_2O_4$ (Cr); Princess Mine, Bancroft, Ontario, Canada sodalite, (Cl); pure vanadium metal SPI 027521-AB 44 Metals Standard Serial AF (V); and pure nickel metal, SPI 027521-AB 44 Metals Standard Serial AF (Ni). Na and K were analyzed using a loss routine to account for any mobilization of the elements under the beam. V Ka and Cr Ka peaks were corrected for potential peak overlap from the Ti Kb and V Kb peaks, respectively. Standard KE-12B, URI and pantelleritic glass was used as the reference standard.

Complementary EPMA analysis was conducted on Bed A and Bed B samples at the Alaskan Volcano Observatory (AVO) at the U.S. Geological Survey in Anchorage, Alaska. The samples were sonicated and sequentially wet-sieved into >125, 63–125, and <63 μm size fractions. Bulk <63 and 63–125 μm separates were mounted in epoxy and sequentially polished to 1 μm with diamond suspension, followed by a 0.1 μm alumina polish step. The coarser 63–125 μm sample grains were carbon coated to 22 nm prior to electron microprobe at the University of Alaska Fairbanks Advanced Instrumentation Laboratory using a JEOL JXA 8530F Electron Microprobe. Methodology followed procedures outlined in Loewen et al. (2022), with uncertainties listed therein. AVO EPMA data for tephra beds A and B are presented in Tables S4 and S6,

while the Brown EPMA data for the Bed B tephra is presented in Table S5.

3.3. Data processing

In this study, we used Principal Component Analysis (PCA) and non-metric multidimensional scaling analysis (nMDS) to understand the relationships among the various major element oxides and quantify the degree of uncertainty in establishing correlations.

PCA determines the principal component (PC); the vector that explains the greatest variance within a multivariate dataset (Wold et al., 1987). Each subsequent PC then describes a sequentially smaller axis of variance oriented orthogonally to the prior component (Zelterman, 2015). When reprojected onto the first and second PCs, the proximity of the data can be used to assess the degree of similarity between the measurements in a multivariate space. We utilized the Scikit-learn package in Python to conduct the PCA analysis (Pedregosa et al., 2011). First, we compared the first PC of major element compositions of Bed A and Bed B with published datasets for regionally relevant tephras, including the Old Crow tephra (Preece et al., 2011), Sheep Creek, Dawson and Variegated tephra (Berger et al., 1996; Jensen et al., 2011; Westgate et al., 2000). Next, we calculated a predictive region (confidence interval = 0.95) using the covariance matrix of the data points of each tephra anchor to investigate the degree of similarity between different tephra anchors (Wickham, 2009). We then utilized the PCs and the predictive regions to establish the degree of similarity between the different tephras.

We also performed non-metric multidimensional scaling (nMDS) analysis using density-based clustering of tephra elemental concentrations. We conducted the nMDS analysis in R using the DBSCAN package (eps = 2, minPts = 5) (Hahsler et al., 2019). We chose nMDS because it does not consider absolute distances between samples and only computes the relative distances between samples (Hammer et al., 2001). More importantly, this approach allows for the identification of outliers that do not belong to any existing cluster. This method is appropriate for this study, as we were concerned with the identification of a potential OCt as well as a potentially unstudied tephra layer.

3.4. Imuruk lake age model

The Imuruk Lake chronology was constructed using multiple approaches, which include accelerator mass spectrometry (AMS) ^{14}C derived ages (measured at the Department of Earth System Science, University of California, Irvine), paleomagnetic techniques, as well as stratigraphic correlation of geochemical proxies and pollen assemblages to other dated successions (Guo et al., 2025).

Initial age constraints were provided by AMS ^{14}C dating on bulk organic matter obtained from 5 samples from the upper 1.5 m of the core, with calibrated dates ranging from present to 50 ka ±0.7 kyr (Table S1). No reservoir correction was applied to the bulk radiocarbon ages beyond the standard calibration with OxCal using Intcal version 20 (Guo et al., 2025; Ramsey and Lee, 2013). This was because low dissolved inorganic carbon concentrations (~1 mg C/L, measured at the Institution of Earth Environment, Chinese Academy of Sciences), an absence of carbonates, well-mixed surface waters, and dominance of in-lake organic matter production collectively suggest minimal influence from old carbon sources. Additional age constraints were provided by six absolutely dated geomagnetic excursions ranging from 70 ka to 240 ka (Guo et al., 2025). Measurements of paleomagnetic inclination were made at regular intervals downcore using a stepwise alternating field (AF) demagnetization of up to 100 mT. Inclination values were calculated after removing secondary overprints, with high-demagnetization steps (>60–80 mT) excluded if they showed noise or non-linear trends. We then evaluated magnetic parameters including NRM/ARM, ARM/IRM, magnetic susceptibility, and mean grain size to distinguish true paleomagnetic excursions from lithologic or diagenetic artifacts. Excursions were identified based on anomalous inclination behavior and cross-validated against global records of geomagnetic excursions within the Brunhes Chron. The Laschamps excursion (~41 ka) was located and its age confirmed by radiocarbon dating in the upper core. Excursions were identified by aligning our magnetic parameters with established global paleomagnetic stacks, including the Norwegian-Greenland Sea (~75 ka), Blake (~123 ka), Albuquerque (~160 ka), Iceland Basin–Biwa I (~194 ka), and Jamaica–Pringle Falls (~213 ka) (Table S2) (Guo et al., 2025). The age uncertainty of these excursions was converted to a single value for input into Bacon by averaging the positive and negative bounds of the reported age ranges.

Here, we adopted the chronology developed by Guo et al. (2025) where major features in the Imuruk Lake Rb/Sr record (a chemical weathering indicator) were aligned with abrupt cooling events, the chronology of which was defined by the composite Chinese Sanbao-Hulu δ^{18}O cave record (Cheng et al., 2009, 2016), under the assumption these climate events were synchronous across the northern hemisphere (Irvalı et al., 2016; Obreht et al., 2020; Salonen et al., 2018). While this assumption could introduce some uncertainty in age estimates, the alignment is consistent with independent stratigraphic evidence. Namely, the Imuruk Rb/Sr record demonstrates orbital scale variability comparable to the Chinese loess Ca/Ti ratio and Lake El'gygytgyn magnetic susceptibility record (Guo et al., 2025), and is also broadly coherent with an Imuruk chronology constrained independently by AMS ^{14}C ages and paleomagnetic excursions. The chronology of the Chinese cave record is derived from absolute U-Th dating with errors less than 2 kyr for the last 450 ka (Cheng et al., 2009, 2016). Here, we take a more conservative approach and assign an uncertainty of ±5 kyr to the Rb/Sr age correlations, based on the maximum reported uncertainty of the Sanbao-Hulu cave record and assuming additional uncertainty in the correlation of Imuruk Rb/Sr to the speleothem δ^{18}O record (Cheng et al., 2009, 2016; Guo et al., 2025).

In this study, we further used these data to assign ages to depth using a Bayesian model (Fig. 4) implemented in Bacon (Blaauw et al., 2021). All AMS^{14}C, paleomagnetic and the Rb/Sr derived tie points were incorporated as age constraints (Tables S1–S3). To estimate the depositional ages of tephras, we extracted the posterior weighted median age from the Bacon Bayesian age–depth model at its stratigraphic depth. Uncertainty was quantified as half the width of the 95 % confidence interval, which we report as a ±value around the median age.

3.5. U1345 age model revision

Recent work (Reyes et al., 2023) have reported OCt bearing detrital shards from IODP Site U1345, with ages constrained by benthic δ^{18}O correlation to that of nearby Site U1343. The δ^{18}O of benthic foraminifera calcite shells is assumed to vary synchronously across sites due to relatively homogenous temperature and salinity variability in the deep ocean (Shackleton, 1967). Site U1345 lies on the Bering shelf margin and its benthic δ^{18}O can be aligned to other North Pacific sites and the global benthic stack (Lisiecki and Raymo, 2005). At Site U1345, while the benthic foraminifera δ^{18}O record (Cook et al., 2016; Reyes et al., 2023) displays a good fit to the global benthic stack (Lisiecki and Raymo, 2005), a ~0.4 ‰ offset at approximately 157 ka implies a potential chronological offset near the assumed timing of the OCt. Despite U1345's high average sedimentation rate of 29–45 cm/kyr (Caissie et al., 2016), the U1345 age model (Reyes et al., 2023) shows a clear chronological gap at the MIS 6 to 5e transition, which suggests the presence of a hiatus. To address this, we developed a revised U1345 age model (Fig. 5, Table S7) anchored to U1343 (Worne et al., 2019), the latter of which is geographically close to U1345, stratigraphically complete, and tuned to the global benthic δ^{18}O chronology (Lisiecki and Raymo, 2005). Eleven tie points were chosen and QAnalySeries (Kotov and Pälike, 2018) to tie U1345's δ^{18}O record to U1343's δ^{18}O record.

4. Results

4.1. Age model

The Imuruk Lake age model was constructed using a total of five radiocarbon dates, six paleomagnetic reversal events and 11 tie points derived from the correlation between Rb/Sr and Sanbao-Hulu $\delta^{18}O$ records (Guo et al., 2025). The model spans the past 0 to 208.6 ka, with the median basal age is estimated as 208.6 ± 5.6 ka (posterior median age ± half of the 95 % confidence interval). Posterior uncertainty increases with depth, ranging from approximately ±1.8 ka at 50 cm to ±5.7 ka at the core base. The average half width of the 95 % confidence interval

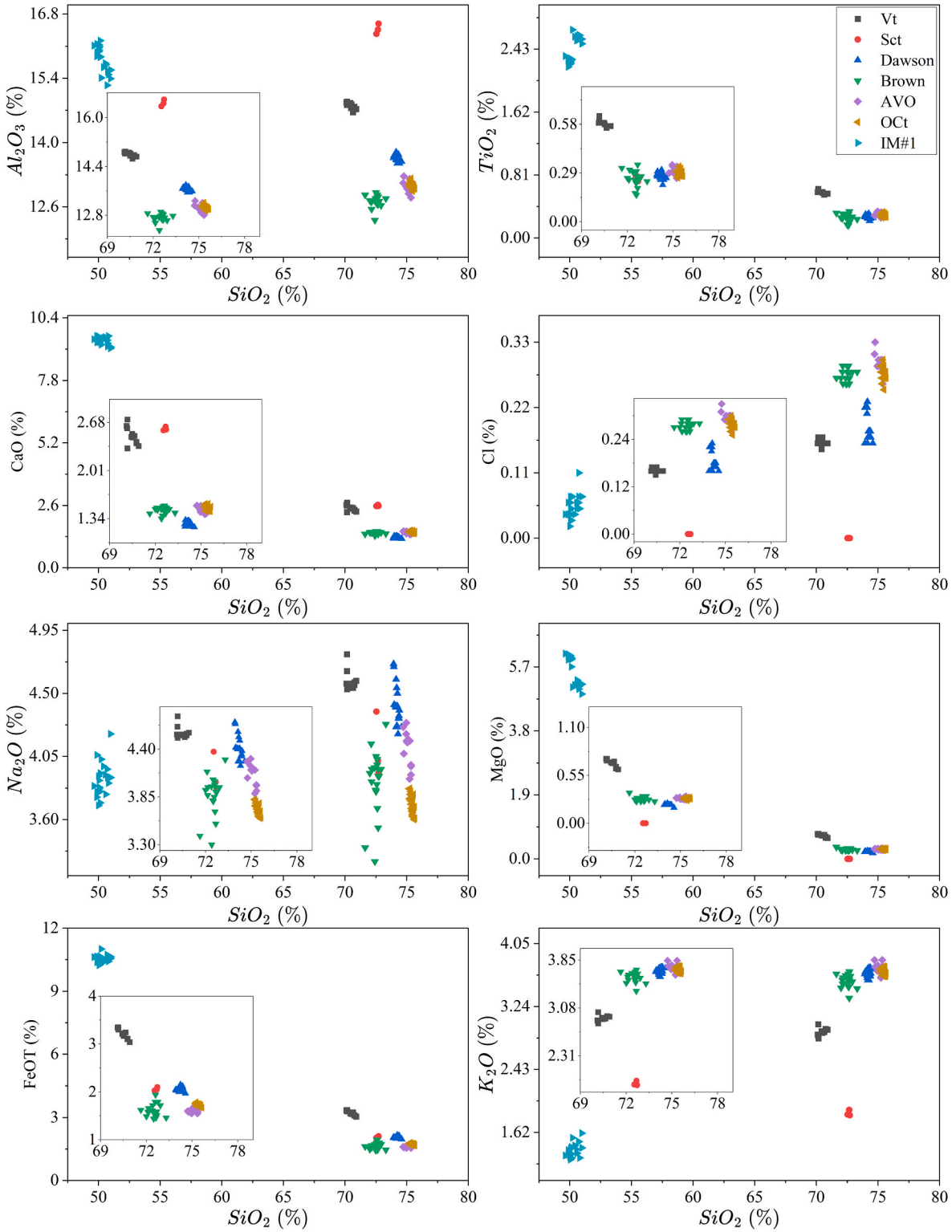


Fig. 2. Harker diagrams comparing major-element glass compositions of IM#1 (Bed A) and Bed B with published Beringian tephras. Inset depicts the Bed B tephra sample against reference rhyolitic tephras. Reference data include OCt (Preece et al., 2011), Dawson (Froese et al., 2002), SCt (Berger et al., 1996), and Vt (Jensen et al., 2011). IM#1 forms a distinct low silica basaltic cluster, whereas Bed B overlaps with published OCt compositions across all major oxides.

width across all modeled depths is ±3.9 ka. The sedimentation rate inferred from the Bacon model cluster around a median of approximately 5.7 cm/kyr. While it is likely that there was variability across glacial–interglacial cycles, the model did not indicate any prolonged hiatuses, erosional unconformities, or major changes in accumulation (Fig. 4). In addition, the Imuruk core consists primarily of laminated dark gray to gray-brown lacustrine muds, with occasional silty intervals. The sequence shows no visible evidence of interrupted sedimentation throughout the 8.8 m record, supporting our interpretation of relatively steady long-term deposition.

4.2. Bed A tephra geochemistry and mineralogy

The Bed A tephra in the Imuruk Lake core is expressed as a distinctive dark brown, double layered ash horizon separated by a thin ~2 mm layer of sediment. The two ash units together are approximately 2 cm thick, with sharp upper and lower contacts in between them. The grains are medium fine ash, dominated by juvenile glass shards. The glass contains abundant plagioclase microlites and minor lithic fragments, consistent with a partially microlithic juvenile population (Fig. S2b).

Major element glass compositions (n = 23) indicate a low silica basaltic chemistry (50.3 ± 0.8 wt % SiO_2), which is distinct from the other regional high silica rhyolitic tephra anchors in Eastern Beringia. Furthermore, The Bed A tephra plots well outside the compositional fields of the Dawson, Sheep Creek, Variegated and Old Crow tephras (Fig. 2).

Bed A therefore represents a previously undocumented local or regional mafic tephra that is distinct from the major late Pleistocene rhyolitic tephras of interior Alaska. We designate this tephra as IM#1. Although IM#1 did not provide any additional age constraints to the Imuruk age model, its stratigraphic position and glass chemistry document previously unrecognized regional eruptive activity.

4.3. Bed B tephra geochemical and lithological characteristics

Bed B tephra is a prominent light gray to white ash layer approximately 2 cm thick, enclosed within the lacustrine sediment with sharp upper and lower contacts. The ash is very well sorted and dominated by fine and highly vesicular glass shards. No sedimentary mixing or reworking was observed.

Microscopic inspection reveals that Bed B consists of homogenous (>90 %) volcanic glass. No phenocrysts or microlites were observed in the grain mounts. Shards display characteristics typical of brittle fragmentation associated with vesicular silicic melt such as thin elongated Y shaped bubble walls. BSE imaging reveals a uniform mid-gray intensity across all shards (Fig. S2c and S2d), with no bright crystalline phases or dark alteration rims. This indicates a chemically homogenous, crystal free rhyolitic glass and minimal post deposition alteration. Minor detrital mineral grains and lithic fragments (<10 %) are sparse.

Major element glass analyses from the Brown university EPMA dataset (n = 20) yield raw SiO_2 values of 72.4 ± 0.7 wt% (2σ), with similarly low variance across other major oxides. Independent analysis from the AVO lab yielded similar results (75.1 ± 0.4 (2σ) wt. % of SiO_2), further demonstrating the homogenous major element chemistry of the Bed B glass population. The offset is consistent with known interlaboratory differences in EPMA beam conditions and standardization (Kuehn et al., 2011), and both datasets occupy a similar high silica rhyolitic composition with overlapping trends in bivariate major oxide space. These results form the basis for the subsequent geochemical comparison of various East Beringian tephra anchors in Fig. 2.

4.4. Principal component analysis

The PCA results indicate that the first two PCs account for 93.9 % of the total variance, with PC1 explaining 81.76 % of the variance (Fig. 3a). The nMDS results also reveal significant geochemical distinctions between the chemical profiles of IM#1 and the Bed B tephra compared with other major Beringian tephra anchors (ANOSIM; R = 0.94, p = 10^{-4}; Fig. 3b).

5. Discussion

5.1. Identification of a new mafic tephra IM#1 from the Imuruk lake record

The major element composition of IM#1 indicates a basaltic, low silica tephra that does not correlate with any of the major late Pleistocene rhyolitic tephra anchors (Dawson, Sheep Creek, Variegated, or Old Crow) discussed in this study. Its low alkali ($K_2O + Na_2O < 5$ wt %) and silica content (≈50 wt%) is characteristic of basaltic magmas (Bas et al., 1986) and consistent with the presence mafic volcanic centers in the Imuruk Lake volcanic field (Mukasa et al., 2007), including nearby vents such as the Camille Cone located approximately 10 km southwest of Imuruk Lake (Mukasa et al., 2007). These eruptions span from the late Miocene to the Holocene but the age of individual flows remain poorly constrained due to low radiogenic Ar contents (K/Ar and $^{40}Ar/^{39}Ar$) (Mukasa et al., 2007). It is possible that the relative position of the Imuruk volcanic field enables the prevailing southwesterlies to transport

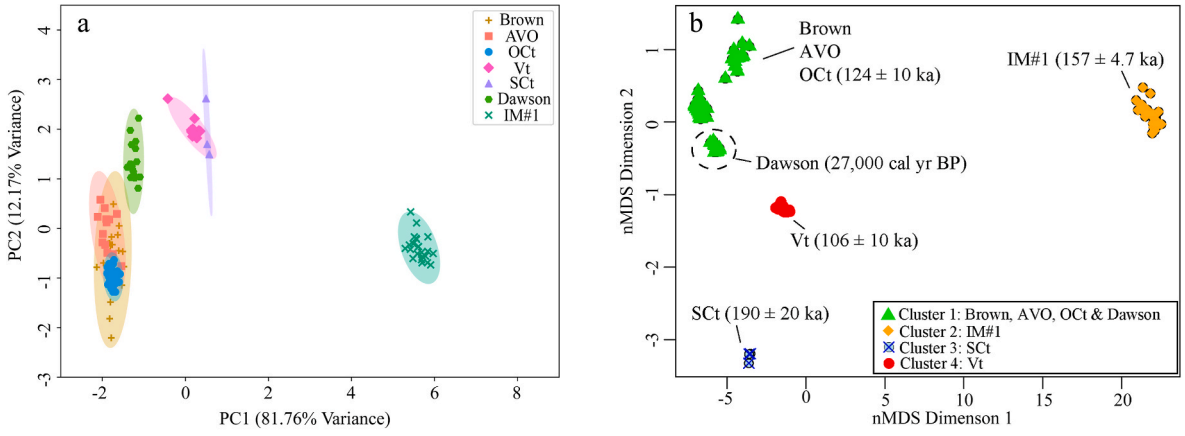


Fig. 3. a) Principal component analysis results of compositional measurements of Beringian tephras and Imuruk Lake tephras. The hypothesized OCt sample (Bed B) analyzed at Brown and AVO showed a high degree of similarity to the OCt documented by Preece et al. (2011); b) Non-metric multidimensional scaling (nMDS) analysis of the compositional data of the hypothesized OCt (Bed B), IM#1 (Bed A), and other Beringian tephra anchors. The Dawson tephra (outlined by the black dashed line) is excluded from Cluster 1 because of its much younger eruption timing at 27,000 cal yr BP.

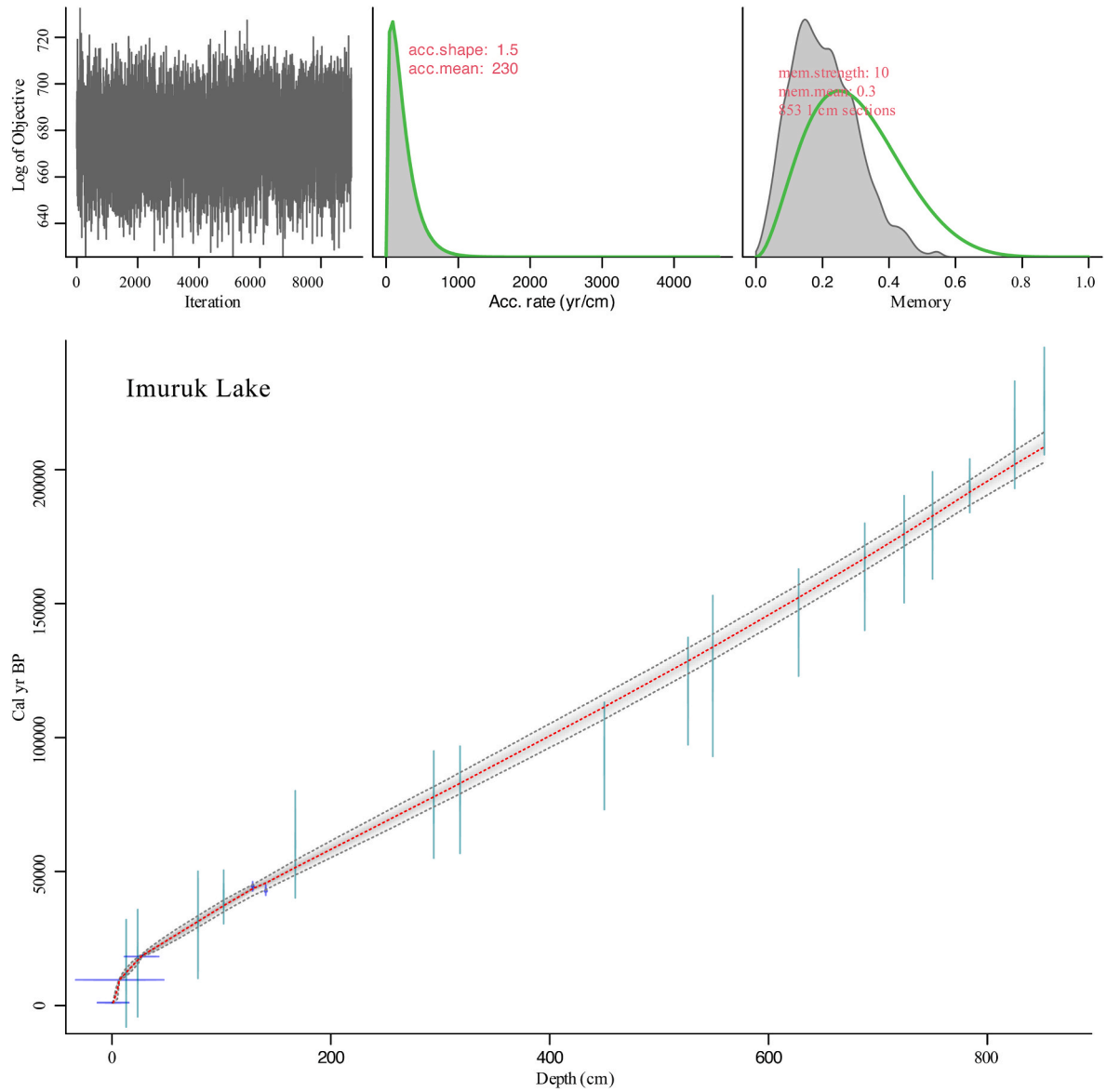


Fig. 4. Imuruk Lake Bayesian age-depth model constructed with Bacon v3.5.2 (Blaauw et al., 2021). Transparent blue symbols show calibrated radiocarbon dates. Stippled lines show 95% confidence intervals, and the red dashed curve represents the best model fit based on the weighted mean age for each depth. Upper panels depict the Markov Chain Monte Carlo (MCMC) iterations (left panel) and prior (green) and posterior (gray histograms) distributions for the accumulation rate (middle) and memory (right panel).

tephra from local eruptions to Imuruk Lake.

Using the Bacon age model and the stratigraphic position of IM#1 between the Blake (125 ± 7.5 ka) and Albuquerque (155 ± 5 ka) geomagnetic excursions (Guo et al., 2025), we estimate the age of IM#1 to be 157.2 ± 4.7 ka. In addition, the double layered structure of IM#1 suggests the possibility of two closely space eruptions rather than a single event. The distinct sediment lamina in between the twin ash layers shows no evidence of grain mixing and therefore suggests that minimal to no sediment reworking occurred post deposition. Based on the age model, the sedimentation rate was calculated as approximately 4.1 cm/kyr, suggesting two closely spaced eruptions occurring ca. 50 years apart.

The PCA and nMDS results confirm that IM#1 is geochemically distinct from other major Beringian tephra examined in this study. IM#1 occupies a separate region that is well outside the compositional clusters defined by the Dawson, Sheep Creek, Variegated and Old Crow tephras. Taken together, the chemistry, stratigraphy and proximity to mafic vents strongly support a local or near regional eruption source. IM#1 thus represents an important new tephrostragraphic marker for mid MIS 6 on the Seward Peninsula in Eastern Beringia.

5.2. *Correlation of Bed B with the Old Crow tephra (OCt)*

In contrast to #IM1, Bed B displays a high silica rhyolitic glass composition that is identical within error to published OCt datasets (Preece et al., 2011). Major element analyses from both Brown and AVO EPMA laboratories fall within the established OCt compositional range, with SiO_2 contents of 72.4 ± 0.7 wt% (Brown) and 75.1 ± 0.4 wt% (AVO). These offsets are consistent with known inter-laboratory differences in EPMA operating conditions (Kuehn et al., 2011). Furthermore, all other major oxides measured for the Bed B tephra show overlapping values with those reported for OCt glass, which confirms a strong geochemical match.

PCA Scores show that Bed B glass population plots within the same compositional cluster as published OCt datasets and is distinct from the Variegated and Sheep Creek tephras (Fig. 3a). The slightly greater

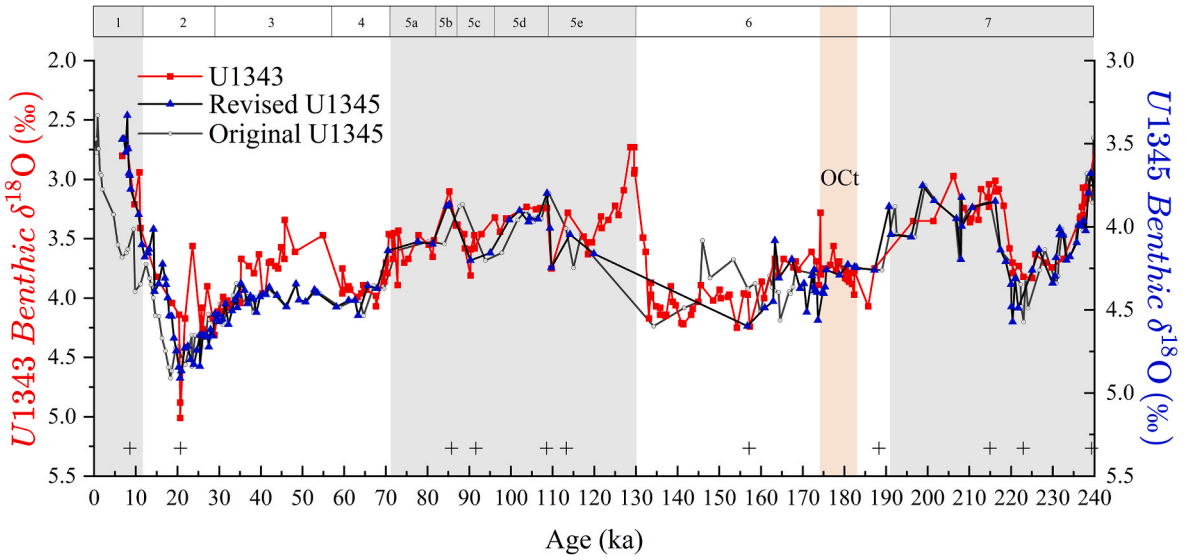


Fig. 5. Revised U1345 age model (blue: U1345 $\delta^{18}O$; red: U1343 $\delta^{18}O$). Eleven tie points (+) were employed to tie U1345 $\delta^{18}O$ (Cook et al., 2016; Reyes et al., 2023) to U1343 $\delta^{18}O$ (Worne et al., 2019). The revised age model now places the marine age of the OCt at ca. 170 ka, slightly younger beyond the chronological uncertainty of Imuruk's OCt age of 179.0 ± 4.6 ka.

spread of the Bed B cluster relative to the reference dataset likely reflects the combined use of two analytical instruments (Brown and AVO), each with small but systematic variation in WDS beam conditions (Kuehn et al., 2011; Loewen et al., 2022). This observed spread did not affect the multivariate clustering of Bed B, which consistently plots within the OCt compositional field The nMDS results support this grouping, with Bed B and OCt forming a coherent multivariate cluster that is separate from other Beringian reference tephras in this study (Fig. 3b). Although the Dawson tephra plots near the OCt cluster due to its high SiO_2 and TiO_2 content (Froese et al., 2002), its independently established age (27,000 cal yr BP) and its incompatibility with the stratigraphic position of the Bed B tephra within the Imuruk age model precludes any correlation.

Chronological constraints from the Imuruk Lake age model further supports the OCt correlation. Bed B lies between the Albuquerque (155 ± 5 ka) and Iceland basin-Biwa I (192 ± 2.5 ka) excursion events (Guo et al., 2025), which provides a robust stratigraphic bracketing that is consistent with independent age estimates for the OCt. Recent work has situated the age of the OCt to within mid MIS 6, with reported ages of 159 ± 8 ka (Reyes et al., 2023). Using the Imuruk Lake Bacon age model and the stratigraphic position of Bed B (735 cm), we refine this placement to 179.0 ± 4.6 ka. This refined age is fully compatible with earlier revised mid MIS 6 age ranges for the OCt. Taken together, the major element geochemistry, PCA results and independent age model constraints provide strong and internally consistent evidence that Bed B represents the OCt in the Imuruk Lake record.

5.3. Other independent evidence for a mid MIS 6 age of the OCt

The Old Crow Tephra has a wide range of published ages. Some paleoecological data suggest that the OCt is older than 124 ± 10 ka (Elias, 2001). For example, climatic interpretations of late Pleistocene beetle fossil assemblages associated with the OCt placed its age at 140 ka (Elias, 2001). However, the oldest age of the beetle in the assemblage was hypothesized to be approximately 150,000 years old. This age was constrained using the mutual climatic range of the beetle fossils, where a warm reconstructed maximum temperature suggests a high summer and winter insolation pattern. Elias (2001) then assigned the 150 ka age by tying it to insolation records in MIS 6.

Recently, the age of the OCt was reported as 159 ± 8 ka based on the appearance of glass shards at Site U1345, representing the first detection of the OCt in a marine sediment core (Reyes et al., 2023). The age model of U1345 was based on the stratigraphic correlation of U1345's benthic foraminiferal $\delta^{18}O$ record and the global benthic $\delta^{18}O$ stack (Lisiecki and Raymo, 2005).

We argue that OCt eruption timing of 159 ± 8 ka is too young, resulting from a misalignment of $\delta^{18}O$ structure. At ca. 157 ka, the benthic foraminifera $\delta^{18}O$ values in the refined U1345 record (Reyes et al., 2023) show an offset of ~0.4 ‰ relative to the global benthic stack (Lisiecki and Raymo, 2005). This mismatch suggests that the previously identified marine age of the OCt shards may be younger than their nominal ages, which is consistent with the terrestrial derived 179.0 ± 4.6 ka age of the OCt from Imuruk Lake. The average sedimentation rate at U1345 is high, but variable, ranging from 29 to 45 cm/kyr (Caissie et al., 2016) with a clear hiatus at the termination of MIS 6 to 5e. To evaluate the depositional age of the OCt horizon in Imuruk Lake independent of the original tuning, we reevaluated the U1345 age model (Fig. 5, Table S7) by comparing the $\delta^{18}O$ record from the site to the U1343 $\delta^{18}O$ record (Worne et al., 2019), the latter of which is in close proximity to U1345, is stratigraphically complete, and is also chronologically tied to the global benthic $\delta^{18}O$ chronology (Lisiecki and Raymo, 2005). The revised U1345 age model displays a good fit to U1343's age model ($R^2 = 0.78$), placing the OCt shards containing interval at approximately 170 ka. Although there is still an offset of ~9 kyr compared to the 179 ka lake-based age, this offset is consistent with the inherent limitation of age modeling at Site U1345. As the site strongly exhibits a variable sedimentation rate (Caissie et al., 2016; Jang et al., 2017; Kender and Kaminski, 2017), this could have introduced age uncertainties on the order of several thousand years when tuning benthic $\delta^{18}O$ to the global stack. Given these constraints, a 9 kyr difference falls within reasonable chronostratigraphic uncertainty for a high latitude marine record.

5.4. Implications of the mid MIS 6 timing of OCt

Our updated eruption age of the OCt at mid-MIS 6 has important implications for the stratigraphic framework, and interpretation of loess-paleosol sequences in Eastern Beringia. At Alaska loess sites, such as the Halfway House, the OCt frequently underlies an organic-rich layer (or thaw unconformity). Previously, the thaw unconformity was thought to represent melting during MIS 5e (Péwé, 1997), as it was one of the warmest interglacial periods of the past two glacial-interglacial cycles (Reyes et al., 2010; Wang and Zong, 2020). Our newly assigned OCt age

of 179.0 ± 4.6 ka corroborates previous interpretations that the thaw unconformity above the OCt at the paleosol sites represents a warming phase with increased productivity during the MIS 5e interglacial.

The stratigraphic position of bison fossils between the OCt and thaw unconformity has been used to constrain the arrival timing of bison into North America to late MIS 6 when the Bering Strait was exposed (Froese et al., 2017). At the Halfway House site, the sediment between the Variegated tephra and the Dawson tephra has a thickness of approximately 4 m (Burgess et al., 2019). Assuming a constant sedimentation rate, this yields an approximate sedimentation rate of 5 cm kyr $^{-1}$. The sediment between the OCt and the organic layer has a thickness of approximately 1.2 m. Using the derived sedimentation rate yielded a much younger OCt age of 147.7 ka. As it is likely that sedimentation was not constant across glacial and interglacial periods, this 147.7 ka age of the OCt likely represents a minimum estimate. This minimum estimate is supported by the marine age of the OCt. As our newly assigned OCt age is in line with a MIS 5e depositional time of the organic thaw layer, our findings reaffirm the late MIS 6 bison migration into east Beringia.

Our study also raises a critical question: Are other major Beringian tephra anchors accurately dated? For example, the Sheep Creek tephra (SCt) is made up of the following stratigraphic units: SCt-F at Fairbanks, Alaska (~200 ka), SCt-CC at Canyon Creek, Alaska, and SCt-K (~80 ka), SCt-A and SCt-C in the western Yukon (Westgate et al., 2008). While SCt-K, A, and C have been determined to have similar ages on the basis of stratigraphy, questions remain regarding the ages of SCt-CC and SCt-F. A source of doubt stems from fossil bones beneath the SCt-CC, yielding a ^{14}C age of 39,360 ± 1740 B.P. (Weber et al., 1981) and a U-series age of 80 ka (Hamilton and Le Bischoff, 1984). However, bison bones are also present in the fossil assemblage, which points to a Rancholabrean land mammal age dating back to MIS 6 (Westgate et al., 2008). Most importantly, it should be noted that SCt-CC was deposited during the Delta Glaciation (Begét and Keskinen, 2003), which occurs stratigraphically below the OCt. Therefore, the SCt-CC must predate the revised OCt age of 179.0 ± 4.6 ka. The SCt-F also occurs stratigraphically below the OCt (~3 m below the OCt layer), and has previously reported thermoluminescence ages of 178 ± 25 ka and 205 ± 31 ka (Berger et al., 1996; Westgate et al., 2008). As these age estimates were in part derived using an earlier OCt age of 140 ± 10 ka (Berger et al., 1996), further work looking into the refinement of the SCt units is warranted.

Moving forward, we recommend that future studies adopt a multiproxy approach when attempting to date tephras. In addition to absolute dating techniques, stratigraphy can also provide a means of constraining the approximate age of tephra. In the case of the OCt, its immediate stratigraphic position below the dark organic-rich thaw unconformity is consistent with that it was the product of MIS 6 deposition instead of MIS 7 (Burgess et al., 2019).

6. Conclusion

This study marks the first time that the OCt has been unambiguously recovered from a terrestrial lacustrine sediment core in Eastern Beringia. The morphology and elemental composition of the OCt from Imuruk Lake are consistent with the OCt layers previously documented in continental loess sediments. Using an independent age model, this study constrains the age of the OCt to 179.0 ± 4.6 ka, approximately 55 kyr older than the canonically established age. This also means that Imuruk Lake is one of the oldest lake sediment records in Eastern Beringia.

Our newly assigned mid-MIS 6 age of the OCt reaffirms the late MIS 6 timing of bison migration into Eastern Beringia. Paleoecological studies utilizing a MIS 6 age of the OCt and an MIS 5e age of the organic rich thaw unconformity will not require a wholesale revision. We also identified a previously undocumented local mafic tephra layer (IM#1), with an age of 157.2 ± 4.7 ka. The eruption that formed IM#1 was characterized by a twin eruption from the same regional crater, occurring approximately 50 years apart. Although IM#1's source caldera is presently unknown, we speculate that it is from the adjacent Imuruk volcanic field.

Based on our revised OCt age, the SCt-F should be older than the OCt given its stratigraphic position below the OCt at multiple sites. This suggests that previously reported ages for the SCt-F (190 ± 20 ka) partly derived from an earlier OCt age of 140 ± 10 ka, may have underestimated its true depositional age. The updated OCt age has profound implications for our understanding of Arctic tephra chronology from the late Middle to Late Pleistocene.

Declaration of competing interest

The authors declare no competing interests.

Acknowledgements

Funding for this project was provided by grants from the National Park Service program (No. P18AC00556-05), Institute at Brown for Environment and Society (IBES) award (No. GR300118), and National Geographic Society grant (No. NGS-55702R-19). We thank Joseph Boesenberg for his assistance with the electron microprobe at Brown University, Ewerton Santos for his assistance in the laboratory, and Matthew Loewen for tephra identification and analysis.

Appendix A. Supplementary data

Supplementary data to this article can be found online at https://doi.org/10.1016/j.quascirev.2026.109816.

Data availability

All data and/or code is contained within the submission.

References

Alexanderson, H., Backman, J., Cronin, T.M., Funder, S., Ingólfsson, Ó., Jakobsson, M., Landvik, J.Y., Löwemark, L., Mangerud, J., März, C., 2014. An arctic perspective on dating mid-late Pleistocene environmental history. Quat. Sci. Rev. 92, 9–31.
Bas, M.L., Maitre, R.L., Streckeisen, A., Zanettin, B., IUGS Subcommission on the Systematics of Igneous Rocks, 1986. A chemical classification of volcanic rocks based on the total alkali-silica diagram. J. Petrol. 27 (3), 745–750.
Begét, J., Edwards, M., Hopkins, D., Keskinen, M., Kukla, G., 1991. Old Crow tephra found at the palisades of the Yukon, Alaska. Quat. Res. 35 (2), 291–297.
Begét, J.E., Keskinen, M.J., 2003. Trace-element geochemistry of individual glass shards of the old Crow tephra and the age of the Delta glaciation, central Alaska. Quat. Res. 60 (1), 63–69.
Berger, G.W., Péwé, T.L., Westgate, J.A., Preece, S.J., 1996. Age of sheep creek tephra (pleistocene) in central Alaska from thermoluminescence dating of bracketing loess. Quat. Res. 45 (3), 263–270.
Blaauw, M., Christen, J.A., Lopez, M.A.A., Vazquez, J.E., Belding, T., Theiler, J., Gough, B., Karney, C., Rcpp, L., Blaauw, M.M., 2021. Package 'Rbacon'. Version.
Bogaard, P.V., Schmincke, H.-U., 1985. Laacher see tephra: a widespread isochronous late Quaternary tephra layer in central and northern Europe. Geol. Soc. Am. Bull. 96 (12), 1554–1571.
Brönnimann, S., Krämer, D., 2016. Tambora and the" Year Without a Summer" of 1816. A perspective on Earth and human systems science. Geographica Bernensia 90.
Burgess, S.D., Coble, M., Vazquez, J.A., Coombs, M.L., Wallace, K.L., 2019. On the eruption age and provenance of the old Crow tephra. Quat. Sci. Rev. 207, 64–79.
Caissie, B.E., Brigham-Grette, J., Cook, M.S., Colmenero-Hidalgo, E., 2016. Bering Sea surface water conditions during marine isotope stages 12 to 10 at Navarin Canyon (IODP site U1345). Clim. Past 12 (9), 1739–1763.
Cheng, H., Edwards, R.L., Broecker, W.S., Denton, G.H., Kong, X., Wang, Y., Zhang, R., Wang, X., 2009. Ice age terminations. Science 326 (5950), 248–252.
Cheng, H., Edwards, R.L., Sinha, A., Spötl, C., Yi, L., Chen, S., Kelly, M., Kathayat, G., Wang, X., Li, X., 2016. The Asian monsoon over the past 640,000 years and ice age terminations. Nature 534 (7609), 640–646.
Cook, M.S., Ravelo, A.C., Mix, A., Nesbitt, I.M., Miller, N.V., 2016. Tracing subarctic Pacific water masses with benthic foraminiferal stable isotopes during the LGM and late Pleistocene. Deep Sea Res. Part II Top. Stud. Oceanogr. 125, 84–95.
Elias, S.A., 2001. Mutual climatic range reconstructions of seasonal temperatures based on late-pleistocene fossil beetle assemblages in Eastern Beringia. Quat. Sci. Rev. 20 (1–3), 77–91.
Froese, D., Stiller, M., Heintzman, P.D., Reyes, A.V., Zazula, G.D., Soares, A.E., Meyer, M., Hall, E., Jensen, B.J., Arnold, L.J., 2017. Fossil and genomic evidence

constrains the timing of bison arrival in North America. Proc. Natl. Acad. Sci. 114 (13), 3457–3462.
Froese, D., Westgate, J., Preece, S., Storer, J., 2002. Age and significance of the late Pleistocene Dawson tephra in eastern Beringia. Quat. Sci. Rev. 21 (20–22), 2137–2142.
Guo, F., Huang, Y., Vachula, R., Wang, K., O'Donnell, J., Du, X., Russell, J., Clemens, S., Yeo, D., Andreev, A., Herzschuh, U., Liu, X., Liu, Y., Su, B., Santos, E., Bobik, T., Yan, M., Sun, Y., Lu, Z., Liu, Z., 2025. Precession and ice sheet control of hydroclimate in Arctic East Beringia over the past 240,000 years [Preprint]. https://doi.org/10.21203/rs.3.rs-4515358/v1.
Hahsler, M., Piekenbrock, M., Doran, D., 2019. dbscan: fast density-based clustering with R. J. Stat. Software 91, 1–30.
Hamilton, T.D., Le Bischoff, J., 1984. EAST-CENTRAL. The United States Geological Survey in Alaska: Accomplishments During 1982 939, 26.
Hammer, Ø., Harper, D.A., Ryan, P.D., 2001. PAST: paleontological statistics software package for education and data analysis. Palaeontol. Electron. 4 (1), 9.
Hopkins, D.M., 1949. Thaw lakes and thaw sinks in the Imuruk Lake area, Seward Peninsula, Alaska. J. Geol. 57 (2), 119–131.
Irvalı, N., Ninnemann, U.S., Kleiven, H.K.F., Galaasen, E.V., Morley, A., Rosenthal, Y., 2016. Evidence for regional cooling, frontal advances, and East Greenland Ice Sheet changes during the demise of the last interglacial. Quat. Sci. Rev. 150, 184–199.
Jang, K., Huh, Y., Han, Y., 2017. Authigenic Nd isotope record of North Pacific Intermediate Water formation and boundary exchange on the Bering Slope. Quat. Sci. Rev. 156, 150–163.
Jensen, B.J., Evans, M.E., Froese, D.G., Kravchinsky, V.A., 2016. 150,000 years of loess accumulation in central Alaska. Quat. Sci. Rev. 135, 1–23.
Jensen, B.J., Preece, S.J., Lamothe, M., Pearce, N.J., Froese, D.G., Westgate, J.A., Schaefer, J., Begét, J., 2011. The variegated (VT) tephra: a new regional marker for middle to late marine isotope stage 5 across Yukon and Alaska. Quat. Int. 246 (1–2), 312–323.
Kender, S., Kaminski, M.A., 2017. Modern deep-water agglutinated Foraminifera from IODP expedition 323, Bering Sea: ecological and taxonomic implications. J. Micropalaeontol. 36 (2), 195–218.
Kotov, S., Pälike, H., 2018. QAnalySeries-a cross-platform time series tuning and analysis tool. AGU Fall Meeting Abstracts.
Kuehn, S.C., Froese, D.G., Shane, P.A., Participants, I.I., 2011. The INTAV intercomparison of electron-beam microanalysis of glass by tephrochronology laboratories: results and recommendations. Quat. Int. 246 (1–2), 19–47.
Lisiecki, L.E., Raymo, M.E., 2005. A pliocene-pleistocene stack of 57 globally distributed benthic δ18O records. Paleoceanography 20 (1).
Loewen, M.W., Lubbers, K., Ruth, J., Izbekov, D., Larsen, P., Jf Graham, N., 2022. Glass electron microprobe analyses methods, precision and accuracy for tephra studies in Alaska.
Longman, J., Gernon, T.M., Palmer, M.R., Manners, H.R., 2021. Tephra deposition and bonding with reactive oxides enhances burial of organic carbon in the Bering Sea. Glob. Biogeochem. Cycles 35 (11).
Lowe, D.J., Shane, P.A., Alloway, B.V., Newnham, R.M., 2008. Fingerprints and age models for widespread New Zealand tephra marker beds erupted since 30,000 years ago: a framework for NZ-INTIMATE. Quat. Sci. Rev. 27 (1–2), 95–126.
Muhs, D.R., Budahn, J.R., 2006. Geochemical evidence for the origin of late Quaternary loess in central Alaska. Can. J. Earth Sci. 43 (3), 323–337.
Mukasa, S.B., Andronikov, A.V., Hall, C.M., 2007. The 40Ar/39Ar chronology and eruption rates of Cenozoic volcanism in the eastern Bering Sea volcanic Province, Alaska. J. Geophys. Res. Solid Earth 112 (B6).
Obreht, I., Wörmer, L., Brauer, A., Wendt, J., Alfken, S., De Vleeschouwer, D., Elvert, M., Hinrichs, K.-U., 2020. An annually resolved record of Western European vegetation response to Younger Dryas cooling. Quat. Sci. Rev. 231, 106198.
Pedregosa, F., Varoquaux, G., Gramfort, A., Michel, V., Thirion, B., Grisel, O., Blondel, M., Prettenhofer, P., Weiss, R., Dubourg, V., 2011. Scikit-learn: machine learning in Python. J. Mach. Learn. Res. 12, 2825–2830.
Péwé, T., Westgate, J., Preece, S., Brown, P., Leavitt, S., 2009. Late Pliocene Dawson cut forest bed and new tephrochronological findings in the Gold Hill Loess, east-central Alaska. Geol. Soc. Am. Bull. 121 (1–2), 294–320.
Péwé, T.L., 1997. Eva Interglaciation Forest Bed, Unglaciated east-central Alaska: Global Warming 125,000 Years ago, vol 319. Geological Society of America.
Pouchou, J.-L., Pichoir, F., 1991. Quantitative analysis of homogeneous or stratified microvolumes applying the model "PAP". In: Electron Probe Quantitation. Springer, pp. 31–75.
Preece, S., Pearce, N.J., Westgate, J., Froese, D., Jensen, B., Perkins, W.T., 2011. Old Crow tephra across eastern Beringia: a single cataclysmic eruption at the close of Marine Isotope Stage 6. Quat. Sci. Rev. 30 (17–18), 2069–2090.
Ramsey, C.B., Lee, S., 2013. Recent and planned developments of the program OxCal. Radiocarbon 55 (2), 720–730.
Reyes, A.V., Froese, D.G., Jensen, B.J., 2010. Permafrost response to last interglacial warming: field evidence from non-glaciated Yukon and Alaska. Quat. Sci. Rev. 29 (23–24), 3256–3274.
Reyes, A.V., Jensen, B.J., Woudstra, S.H., Bolton, M.S., Buryak, S.D., Cook, M.S., Harvey, J., Westgate, J.A., 2023. Detrital glass in a Bering Sea sediment core yields a ca. 160 ka Marine Isotope Stage 6 age for old Crow tephra. Geology 51 (1), 106–110.
Salonen, J.S., Helmens, K.F., Brendryen, J., Kuosmanen, N., Väliranta, M., Goring, S., Korpela, M., Kylander, M., Philip, A., Plikk, A., 2018. Abrupt high-latitude climate events and decoupled seasonal trends during the Eemian. Nat. Commun. 9 (1), 2851.
Shackleton, N., 1967. Oxygen isotope analyses and Pleistocene temperatures re-assessed. Nature 215 (5096), 15–17.
Stothers, R.B., 1984. The great Tambora eruption in 1815 and its aftermath. Science 224 (4654), 1191–1198.
Strauss, J., Schirrmeister, L., Mangelsdorf, K., Eichhorn, L., Wetterich, S., Herzschuh, U., 2015. Organic-matter quality of deep permafrost carbon – a study from Arctic Siberia. Biogeosciences 12 (7), 2227–2245.
Vachula, R.S., Huang, Y., Longo, W.M., Dee, S.G., Daniels, W.C., Russell, J.M., 2019. Evidence of Ice Age humans in eastern Beringia suggests early migration to North America. Quat. Sci. Rev. 205, 35–44.
Walter, R.C., 1989. Application and limitation of fission-track geochronology to Quaternary tephras. Quat. Int. 1, 35–46.
Wang, M., Zong, Y., 2020. Significant SST differences between peak MIS5 and MIS1 along the low-latitude western North Pacific margin. Quat. Sci. Rev. 227, 106060.
Weber, F.R., Hamilton, T.D., Hopkins, D.M., Repenning, C.A., Haas, H., 1981. Canyon Creek: a late Pleistocene vertebrate locality in interior Alaska. Quat. Res. 16 (2), 167–180.
Westgate, J., Walter, R., Pearce, G., Gorton, M., 1985. Distribution, stratigraphy, petrochemistry, and palaeomagnetism of the late Pleistocene old Crow tephra in Alaska and the Yukon. Can. J. Earth Sci. 22 (6), 893–906.
Westgate, J.A., Hamilton, T.D., Gorton, M.P., 1983. Old Crow tephra: a new late Pleistocene stratigraphic marker across north-central Alaska and Western Yukon Territory. Quat. Res. 19 (1), 38–54.
Westgate, J.A., Preece, S., Froese, D.G., Pearce, N.J., Roberts, R., Demuro, M., Hart, W., Perkins, W., 2008. Changing ideas on the identity and stratigraphic significance of the sheep Creek tephra beds in Alaska and the Yukon Territory, northwestern North America. Quat. Int. 178 (1), 183–209.
Westgate, J.A., Preece, S.J., Kotler, E., Hall, S., 2000. Dawson tephra: a prominent stratigraphic marker of late Wisconsinan age in west-central Yukon, Canada. Can. J. Earth Sci. 37 (4), 621–627.
Westgate, J.A., Stemper, B.A., Péwé, T.L., 1990. A 3 my record of Pliocene-Pleistocene loess in, interior Alaska. Geology 18 (9), 858–861.
Wickham, H., 2009. Elegant graphics for data analysis (ggplot2). Applied Spatial Data Analysis R.
Wold, S., Esbensen, K., Geladi, P., 1987. Principal component analysis. Chemometr. Intell. Lab. Syst. 2 (1–3), 37–52.
Worne, S., Kender, S., Swann, G.E., Leng, M.J., Ravelo, A.C., 2019. Coupled climate and subarctic Pacific nutrient upwelling over the last 850,000 years. Earth Planet Sci. Lett. 522, 87–97.
Zelterman, D., 2015. Applied Multivariate Statistics with R. Springer.